Coriolis-Coupled Wave Packet Dynamics of H + HLi Reaction

R. Padmanaban and S. Mahapatra*

School of Chemistry, University of Hyderabad, Hyderabad, 500 046, India

Received: December 13, 2005; In Final Form: March 11, 2006

We investigated the effect of Coriolis coupling (CC) on the initial state-selected dynamics of H + HLi reaction by a time-dependent wave packet (WP) approach. Exact quantum scattering calculations were obtained by a WP propagation method based on the Chebyshev polynomial scheme and ab initio potential energy surface of the reacting system. Partial wave contributions up to the total angular momentum $J = 30$ were found to be necessary for the scattering of HLi in its vibrational and rotational ground state up to a collision energy ~0.75 eV. For each J value, the projection quantum number K was varied from 0 to min (J, K_{max}), with $K_{max} = 8$ until $J = 20$ and $K_{max} = 4$ for further higher J values. This is because further higher values of K do not have much effect on the dynamics and also because one wishes to maintain the large computational overhead for each calculation within the affordable limit. The initial state-selected integral reaction cross sections and thermal rate constants were calculated by summing up the contributions from all partial waves. These were compared with our previous results on the title system, obtained within the centrifugal sudden and J-shifting approximations, to demonstrate the impact of CC on the dynamics of this system.

I. Introduction

In this article, we present a detailed full-dimensional quantum wave packet (WP) dynamical calculations of the integral reaction cross section and thermal rate constant for the H + HLi scattering. These two quantities represent the most important dynamical observables of a chemical reaction.[1] The reaction cross section is calculated by summing up all partial wave contributions of the total angular momentum J to the reaction probability. A further averaging of the energy-dependent reaction cross sections at a given temperature yields the thermal rate constant. In an atom−diatom reactive scattering, the reaction probability for $J \neq 0$ is best obtained by carrying out the explicit quantum dynamical simulations[2] which involve 4 degrees of freedom−3 to describe the relative orientation of the atom and diatom in a plane and the fourth one, the projection K of the total angular momentum J, defining the orientation of this plane. A commonly employed approach in the body-fixed (BF) frame is called the centrifugal sudden or the coupled states (CS) approximation,[3,4] in which K is a good quantum number and is treated as a fixed parameter. This reduces the dimensionality of the problem to three. We used this approximation for the title reaction in our previous publication[5] and the results will be discussed here in relation to the present and more exact Coriolis coupling (CC) results. In the latter the neighboring K states couple each other and thereby the dimensionality of the problem becomes four. Recently, similar studies on the effect of CC terms on bimolecular reactive scattering systems have also been treated in the literature.[6,7]

The H + HLi collision proceeds via three dynamical paths; (i) a highly exothermic (exothermicity ~ 2.09 eV[8]) depletion path; H + HLi → H_2 + Li (R1), (ii) a thermoneutral exchange path; H + HLi → HLi + H (R2), and (iii) a nonreactive path; H + HLi → H + HLi (NR). A study of the collision dynamics of HLi molecule is particularly relevant in a better understanding of the primordial lithium chemistry.[9−11] The formation and depletion of HLi and its ionic counterparts play crucial roles in the Stellar evolution and galactic lithium production.[12] Moreover, the existence of these molecular species may cause significant anisotropy of the cosmic background radiation by undergoing Thompson scattering with the emitted photon.[13] The minimum energy path of the reactive processes R1 and R2 occurs at the collinear configuration of the three nuclei. The potential energy surface (PES) for the ground electronic state of the H + HLi system is reported for the collinear configuration by Clarke et al.[14] and for the three-dimensional configuration by Dunne, Murrell, and Jemmer (DMJ)[8] and by Kim et al.[15] In addition to describing the PES in the collinear configuration, Clarke et al.[14] have also calculated the initial state-selected reaction probabilities by a quasiclassical trajectory (QCT) as well as by a time-dependent WP approach. Their findings revealed an early barrier (~0.036 eV) and a strong exothermicity of ~ 2.0238 eV for the HLi depletion path (R1).[14] The existence of such a barrier is not found in the three-dimensional PESs reported by Dunne et al.[8] and Kim et al.;[15] however, the exothermicity of the depletion reaction is found to be consistent with the results of Clarke et al.[14] DMJ PES[8] is an analytical representation of the ab initio potential-energy data computed by the authors including the configuration interaction and using an augmented correlation-consistent valence double-ζ basis set. We used this PES in present dynamical study. Kim et al.[15] have performed the complete-active space self-consistent-field calculations to obtain the potential energy data in three-dimensional arrangements of the nuclei. These authors have performed quasi classical trajectory calculations and reported the direct nature of the HLi depletion path and found that the reaction dynamics is insensitive to internal excitation of the reagent HLi.

In our previous studies,[5,16,17] we have investigated dynamics of H + HLi collisions on the DMJ PES by a time-dependent WP approach. We reported the reaction probabilities for the exchange as well as the depletion channel for the total angular momentum $J = 0$.[16] The oscillations in the energy dependence

* Corresponding author. E-mail: smsc@uohyd.ernet.in. Fax: +91-40-23012460.

10.1021/jp057280v CCC: $33.50
Published on Web 04/14/2006

of reaction probabilities are identified with the resonances of the system and subsequently these are calculated by a pseudospectral approach.[17] These resonances are characterized in terms of their eigenfunctions and lifetimes. We found that some of the resonances can survive as long as $\sim$ 250 fs.[17] We have also carried out dynamical calculations for $J \neq 0$[5] using the CS[3,4] as well as *J*-shifting (JS)[18,19] approaches and reported integral reaction cross sections and temperature-dependent rate constants for both the exchange and depletion channels.[5] Our findings reveal a preference of the exchange channel over the depletion channel at low and moderate collision energies; however, at high energies the depletion channel is preferred. The resonance oscillations seen in the reaction probability curves average out with many partial wave contributions in the integral reaction cross section results.[5]

Very recently Defazio et al.[20] reported the thermal product distributions, rate constants and mechanisms of H + HLi reaction by employing the real WP method[21] and the JS[18] approximation. Their findings reveal that the LiH depletion (R1) rate is larger than the H-exchange (R2) rate (up to $\sim$ 40 K) and the latter preponderates at higher temperatures. The rate constant results for both the processes are reported to deviate from the Arrhenius type of behavior. In this study, we report the initial state-selected integral reaction cross sections and temperature-dependent rate constants for the R1 and R2 channels and discuss the effect of CC[3,6,7,23−25] on these dynamical quantities. Our findings reveal that inclusion of the partial-wave contribution up to $J = 30$ is necessary for the reaction cross sections up to a collision energy of $\sim$0.75 eV. The projection quantum number *K* up to 8 (up to $J = 20$) and 4 (for further higher *J* values) is included in the dynamics. The dynamical results show that the R2 channel is generally preferred over the R1 channel. The thermal rate constants for both the R1 and R2 channels monotonically increase with temperature. The Coriolis coupling leads to an increase of the reaction rate at low temperatures and a decrease at high temperatures, when compared to the CS results for both the channels. Deviation from the Arrhenius type of behavior is observed for the rate constant results of both the channels. The essential details of the theoretical method to treat the scattering dynamics are outlined in section II. The results are reported, discussed, and compared with those obtained from a reduced dimensionality treatment in section III. Finally, the summarizing remarks are presented in section IV.

II. Theoretical Framework

The nuclear dynamical simulations are carried out employing a time-dependent WP approach and the integral cross sections and thermal rate constants of the H + HLi reaction are calculated. The time-dependent Schrödinger equation (TDSE) is numerically solved on each grid. For an explicitly time-independent Hamiltonian, the solution of the TDSE is given by

$$|\Psi(t)\rangle = \exp\left[-i\hat{H}\frac{t}{\hbar}\right]|\Psi(t=0)\rangle \qquad (1)$$

where $|\Psi(t=0)\rangle$ and $|\Psi(t)\rangle$ are the wave functions at time zero and *t*, respectively, and $\hat{H}$ is the Hamiltonian operator of the reacting system.

A. The Hamiltonian and the Initial Wave Function. The Hamiltonian operator $\hat{H}$ in eq 1 is expressed for the H + HLi collisional system in terms of the mass-scaled reactant channel BF Jacobi coordinates *R* (the distance of H from the center-of-mass of the HLi molecule), *r* (the HLi internuclear distance) and γ (the angle between $\vec{R}$ and $\vec{r}$) as follows[3,26,27]

$$\hat{H} = -\frac{\hbar^2}{2\mu}\left[\frac{\partial^2}{\partial R^2} + \frac{\partial^2}{\partial r^2}\right] + \frac{\hat{j}^2}{2\mu r^2} + \frac{\hat{l}^2}{2\mu R^2} + V(R, r, \gamma) \qquad (2)$$

where $\mu = \sqrt{m_H{}^2 m_{Li}/(2m_H + m_{Li})}$, ($m_H$ and m_{Li} are the masses of H and Li, respectively) is the three-body reduced mass. $\hat{j}$ denotes the rotational angular momentum operator of HLi, and $\hat{l}$ denotes the orbital angular momentum operator. The quantity $\hat{l}^2$ can be expressed as

$$\hat{l}^2 \equiv (\hat{J} - \hat{j})^2 = \hat{J}^2 + \hat{j}^2 - 2\hat{J}_z\hat{j}_z - \hat{J}_+\hat{j}_- - \hat{J}_-\hat{j}_+ \qquad (3)$$

where $\hat{J}$ is the total angular momentum operator describing the three-body rotation and $\hat{J}_z$ and $\hat{j}_z$ are the respective BF *z* components. $\hat{J}_+(\hat{J}_-)$ and $\hat{j}_+(\hat{j}_-)$ are the corresponding raising (lowering) operators, $V(R, r,\gamma)$ is the interaction potential of the H + HLi system. The DMJ PES of H + HLi[8] is used for the latter in the following study.

The physical wave function of the H + HLi system satisfying the TDSE [eq 1] and depending on the total angular momentum *J*, its projection onto the space-fixed (SF) *z*-axis, *M*, and parity under inversion of nuclear coordinates in the SF frame, *p*, can be expanded in terms of BF Jacobi coordinates (R, r,γ) and three Euler angles ($\omega \equiv \theta\phi\delta$) as[2−4,24,25]

$$|\Psi^J_M(R, r,\gamma,\omega, t)\rangle = \frac{1}{Rr}\sum_{K=-J}^{J} F^{Jp}_{KM}(\omega)|\Psi^J_K(R, r,\gamma, t)\rangle \qquad (4)$$

where *K* is the projection of $\boldsymbol{j}$ (and also of $\boldsymbol{J}$) on the BF *z* axis. $F^{Jp}_{KM}(\omega)$ denotes the normalized parity-adapted angular functions written in terms of the Wigner rotation matrix elements, D^J_{KM}, as[28,29]

$$F^{Jp}_{KM}(\omega) = [2(1 + \delta_{K,0})]^{-1/2}\sqrt{\frac{2J+1}{8\pi^2}}\,[D^J_{K,M}(\omega) + (-1)^{J+K+p}D^J_{-K,M}(\omega)] \qquad (5)$$

where $D^J_{-K,M}(\omega) = (-1)^K D^J_{K,M}(\omega)$. These matrix elements are expressed in the passive *zyz* convention for rotation.[23,30] The parity selection depends on the odd or even values of *J* and *K* is restricted to non negative values. For instance, odd *J* states will have odd parity ($p = 1$) and even *J* states will have even parity ($p = 0$). In case of $J = 2$, for example, the dynamical calculations are carried out for each *K* values varying from 0 to 2 (note that the $(-1)^K$ term is also there in the expansion of $D^J_{-K,M}(\omega)$) and even value of parity ($p = 0$).

In this study, we consider the collisions of H with HLi in its vibrational and rotational ground state ($v_i = 0$, $j_i = 0$). Substituting the Hamiltonian [eq 2], and the wave function [eq 4], in the TDSE, after some algebra the effective Hamiltonian in the BF frame operating on Ψ^J_K is obtained in a tridiagonal matrix form as[3,4]

$$\hat{H} = \left[-\frac{\hbar^2}{2\mu}\left(\frac{\partial^2}{\partial R^2} + \frac{\partial^2}{\partial r^2}\right) - \frac{\hbar^2}{2I}\left(\frac{1}{\sin\gamma}\frac{\partial}{\partial\gamma}\sin\gamma\frac{\partial}{\partial\gamma} - \frac{K^2}{\sin^2\gamma}\right) + \frac{\hbar^2}{2\mu R^2}[\hat{J}^2 - 2K^2] + V(R, r,\gamma)\right]\delta_{K,K'} - \frac{\hbar^2}{2\mu R^2}\left[C^+_{JK}\left(\frac{\partial}{\partial\gamma} - K\cot\gamma\right)\delta_{K,K'+1} + C^-_{JK}\left(-\frac{\partial}{\partial\gamma} - K\cot\gamma\right)\delta_{K,K'-1}\right] \qquad (6)$$

where $I = \mu R^2 r^2/(R^2 + r^2)$, is the three-body moment of inertia

and, $C_{JK}^{\pm} = [J(J+1) - K(K \pm 1)]^{1/2}$.[29] The last two off-diagonal terms in eq 6, couple the various neighboring K-states (i.e., K with $K \pm 1$) in the BF frame and represent the CC terms. In the CS approximation these terms are neglected. Therefore, in addition to the three BF coordinates, wave function also depends on K adding to the overall dimensionality of the quantum dynamical treatment. Hereafter, we refer the first term in the right-hand side of eq 6 as $\hat{T}(R, r)$, the second and third terms as $\hat{T}_{dia}(\gamma)$, and the fifth and sixth terms as $\hat{T}_{off}(\gamma)$.

The initial WP $|\Psi_K^J(R, r, \gamma, t = 0)\rangle$ is prepared in the asymptotic reagent channel (occurring at $R \rightarrow \infty$), where the interaction potential vanishes. In such a situation it can be described as a product of translational wave function $F(R)$ for the approach of H to the center-of-mass of HLi, the rovibrational wave function $\phi_{vj}(r)$ of the HLi molecule and the $\mathcal{L}^2$-normalized associated Legendre polynomial, $\tilde{P}_j^K(\cos\gamma)$ for the motion along the approach angle γ:

$$|\Psi_K^J(R, r, \gamma, t = 0)\rangle = F(R)\phi_{vj}(r)\tilde{P}_j^K(\cos\gamma) \quad (7)$$

We choose a minimum uncertainty Gaussian wave packet (GWP) for $F(R)$:

$$F(R) = \left(\frac{1}{2\pi\delta^2}\right)^{1/4} \exp\left[-\frac{(R - R_0)^2}{4\delta^2} - ik_0(R - R_0)\right] \quad (8)$$

The quantity δ is the width parameter of the GWP, and R_0 and k_0 correspond to the location of its maximum in the coordinate and momentum spaces, respectively.

The function $\phi_{vj}(r)$ represents the rovibrational eigenfunction corresponding to a given vibrational v and rotational j state of the reagent HLi molecule. The function $\phi_{vj}(r)$ is obtained by solving the eigenvalue equation

$$\left[-\frac{\hbar^2}{2\mu'}\frac{d^2}{dr'^2} + V(r') + \frac{j(j+1)\hbar^2}{2\mu' r'^2}\right]\phi_{vj}(r') = \epsilon_{vj}\phi_{vj}(r') \quad (9)$$

Here μ' is the reduced mass of HLi, ϵ_{vj} is the energy eigenvalue and, $r' = r(\mu/\mu')^{1/2}$ is the unscaled internuclear distance of the HLi molecule. $V(r')$ is the potential energy of HLi obtained from the DMJ PES[8] by setting $R \rightarrow \infty$. We used the sine-discrete variable representation (DVR) method of Colbert and Miller[31] to solve the above eigenvalue equation.

B. Wave Packet Propagation. The action of the time-evolution operator $\exp[-i\hat{H}t/\hbar]$ on the WP [eq 1] is carried out numerically by dividing the time axis into N segments of length Δt. The time-evolution operator is approximated by a Chebyshev polynomial (CP) expansion scheme, originally proposed by Tal-Ezer and Kosloff.[32] In this scheme, the time evolution operator is expressed as

$$\exp[-i\hat{H}\Delta t/\hbar] = \exp(-i\bar{H}\Delta t/\hbar)\exp(-i\alpha\hat{H}_{norm}) \quad (10)$$

where $\hat{H}_{norm} = 2(\hat{H} - \bar{H})/\Delta E$, with, $\bar{H} = (E_{max} + E_{min})/2$, and, $\Delta E = E_{max} - E_{min}$. The quantity H_{norm} represents the scaled Hamiltonian with eigenvalues in $(-1,1)$.

The first term in the right-hand side of eq 10 represents the phase shift due to a shift of the energy scale (as stated above) and the second term is approximated by the CP series (with the Bessel functions J_n of first kind and the Chebyshev polynomials Φ_n) as

$$\exp(-i\alpha\hat{H}_{norm}) = \sum_{n=0}^{\infty}(2 - \delta_{n0})J_n(\alpha)\Phi_n(-i\hat{H}_{norm}) \quad (11)$$

The functions $\Phi_n(-i\hat{H}_{norm})$ are the complex CPs of order n satisfying the recursion relation

$$\Phi_{n+1} = -2i\hat{H}_{norm}\Phi_n + \Phi_{n-1} \quad (12)$$

with $\Phi_0 = 1$ and $\Phi_1 = -i\hat{H}_{norm}$. The number of CP terms to be used in the above expansion [in eq 11] is determined by the volume of the time-energy phase space, $\alpha = \Delta E\Delta t/2\hbar$.

The action of the radial $\hat{T}(R, r)$ and the angular $\hat{T}(\gamma)$ kinetic energy operators on the wave function are carried out using the fast Fourier transform (FFT) method[33] and a DVR method,[34,35] respectively. For the latter, the choice of the grid along γ, in principle depends on the J and K values. In practice, the choice of different γ grid in a single numerical calculation is impossible. To avoid this difficulty, we used the grid points corresponding to $J = 0$ and $K = 0$ throughout the calculations, however, we used appropriate eigenvector matrix corresponding to a particular K value (by diagonalizing the cos γ operator in the basis of the associated Legendre polynomials) to set up the DVR-finite basis representation (FBR) transformation matrix.[26,34] In the following, the nodes of a 48-points Gauss Legendre quadrature (GLQ)[36] are used for the grid points along γ.

The coordinate grid consists of equally spaced points R_l and r_m along the two Jacobi distances R and r, respectively. The initial wave function at each node (R_l, r_m, γ_n) of this grid is given by

$$|\Psi_K^J(R_l, r_m, \gamma_n, t = 0)\rangle = |\Psi_{lmn}\rangle = \sqrt{w_n}\, F(R_l)\phi_{vj}(r_m)\tilde{P}_j^K(\cos\gamma_n) \quad (13)$$

The action of the rotational kinetic energy operator is then carried out by transforming the DVR wave function [eq 13] to the angular momentum space (FBR), multiplying it by the diagonal/ off-diagonal value of the operator $T(\gamma)$, and transforming it back to the DVR representation. Numerically, this is accomplished in a single step as follows

$$\hat{T}_{dia}(\gamma)|\Psi_{lmn'}^K\rangle = \sum_n\left\{\sum_j \boldsymbol{U}_{n',j}^{K\,\dagger}\left\{\frac{\hbar^2}{2}\left[\frac{j(j+1)}{I} + \frac{J(J+1) - 2K^2}{\mu R^2}\right]\right\}\boldsymbol{U}_{j,n}^K\right\}|\Psi_{lmn}^K\rangle \quad (14)$$

$$\hat{T}_{off}^{\pm}(\gamma)|\Psi_{lmn'}^K\rangle = \sum_n\left\{\sum_j \boldsymbol{U}_{n',j}^{K\pm1\dagger}\left\{\frac{\hbar^2}{2\mu R^2}[C_{J\,K}^{\pm}\, C_{jK}^{\pm}]\right\}\boldsymbol{U}_{j,n}^K\right\}|\Psi_{lmn}^{K\pm1}\rangle \quad (15)$$

where the quantity $\boldsymbol{U}_{j,n}$ represents the DVR−FBR transformation matrix and $\boldsymbol{U}_{n,j}^{\dagger}$ is the Hermitian conjugate to $\boldsymbol{U}_{j,n}$. $C_{JK}^{\pm}$ and $C_{jK}^{\pm}$ are the CC terms.

In dynamical studies involving scattering systems, as the WP moves forward in time, its fast moving components approach the grid boundaries and are no longer relevant for the rest of the dynamics. Therefore, to avoid unphysical reflections or wrap around of these components from the boundaries of a finite sized grid, the WP at each time step is multiplied by a damping function[37]

$$f(X_i) = \sin\left[\frac{\pi}{2}\frac{(X_{mask} + \Delta X_{mask} - X_i)}{\Delta X_{mask}}\right], \quad X_i \geq X_{mask} \quad (16)$$

which is activated in the asymptotic reactant and product channels. X_{mask} is the point at which the damping function is initiated and $\Delta X_{mask}(=X_{max} - X_{mask})$ is the width of X over which

the function decays from 1 to 0, with X_{max} being the maximum value of X in that direction, in a particular channel. The stability and numerical convergence of the CP scheme is explicitly checked with respect to the above damping function.

C. Final Analysis: Reaction Cross Section and Thermal Rate Constant. The initial-state selected and energy-resolved reaction probabilities corresponding to a given value of J and $K = 0 - min(J, K_{max})$ are obtained by integrating the reactive flux of the WP at a dividing surface at $r = r_d$, in the specific reaction channel (R1 or R2).

$$P_i^{JK}(E) = \sum_f |S_{fi}^{JK}|^2 = \langle \Phi(R, r, \gamma, E)|\, \hat{F} |\Phi(R, r, \gamma, E)\rangle|_{r=r_d} \tag{17}$$

where S_{fi}^{JK} is the reactive scattering matrix from an initial state i of the reactant to a final state f of the product. The flux operator $\hat{F}$ in terms of the dividing surface (at $r = r_d$) can be given as[38,39]

$$\hat{F} = -\frac{i\hbar}{2\mu}\left[\frac{\partial}{\partial r}\delta(r - r_d) + \delta(r - r_d)\frac{\partial}{\partial r}\right] \tag{18}$$

With this, the reaction probability in eq 17 can be expressed as

$$P_i^{JK}(E) = \frac{\hbar}{\mu} Im\left[\left\langle \Phi(R, r_d, \gamma, E)\middle|\frac{\partial \Phi(R, r_d, \gamma, E)}{\partial r}\right\rangle\right] \tag{19}$$

The quantity in the right-hand side of the above equation is integrated over the entire range of R and γ. The quantity E represents the total energy (relative translational + rovibrational) of the collisional system. The energy normalized time-independent reactive scattering wave function is calculated along the dividing surface at $r = r_d$ as

$$|\Phi(R, r_d, \gamma, E)\rangle = |\psi(R, r_d, \gamma, E)\rangle/\kappa_E \tag{20}$$

The energy-dependent wave function $\psi(R, r_d, \gamma, E)$ is obtained by Fourier transforming the time-evolved WP, $\Psi(R, r, \gamma, t)$ along the dividing surface. The quantity k_E is the weight of the translational energy component contained in the initial WP for a given total energy E

$$\kappa_E = \left(\frac{\mu}{2\pi\hbar k_{vj}}\right)^{1/2} \int_{-\infty}^{+\infty} F(R) e^{ik_{vj}R}\, dR \tag{21}$$

where $k_{vj} = \sqrt{2\mu(E-\epsilon_{vj})/\hbar}$, with ϵ_{vj} being the initial rovibrational energy of the HLi molecule.

The distinction between the two channels (R1 and R2) in the product asymptote is made by comparing the internuclear distances of the product H_2 and HLi molecules. The reactive flux, [eq 18], in which the H_2 distance is smaller than the HLi distance is considered to represent the (R1) channel and the rest is considered to represent the (R2) channel.[40]

The reaction probabilities depending upon J, K and p [cf. eq 19] are then summed up with appropriate weight for a specified (v, j) state. This yields the cumulative reaction probability (CRP)[2]

$$N_{vj}(E) = \frac{1}{2j+1}\sum_{K=0}^{K_{max}}\sum_{J\geq K}^{J_{max}}(2J+1)P_{vj}^{JK}(E) \tag{22}$$

The initial state-selected integral reaction cross section for a specified initial (v, j) state of HLi is then calculated from

$$\sigma_{vj}(E) = \frac{\pi}{k_{vj}^2} N_{vj}(E) \tag{23}$$

The initial state-specific thermal rate constant can be calculated from the CRP as[38]

$$k(T) = (2\pi\hbar Q_R(T))^{-1} \int_{-\infty}^{+\infty} dE\, e^{-E/k_BT} N_{vj}(E) \tag{24}$$

the quantity $Q_R(T)$ in the above equation defines the reagent H+HLi partition function, $Q_R(T) = Q_{ele}Q_{tr}Q_{vib}Q_{rot}$.[41] In the present case

$$Q_{ele} = 1 \tag{25a}$$

$$Q_{tr} = \left(\frac{2\pi m k_B T}{\hbar^2}\right)^{3/2} \tag{25b}$$

$$Q_{vib} = \frac{1}{1 - \exp\left(-\frac{h\nu}{k_B T}\right)} \tag{25c}$$

$$Q_{rot} = \sum_j^{\infty}(2j+1)\exp(-j(j+1)B/k_BT) \tag{25d}$$

are the electronic, translational, vibrational and rotational contribution to the partition function, respectively. Here, B is the rotational constant of HLi molecule (~ 7.5131 cm^{-1}),[8] and k_B is the Boltzmann constant.

D. Computational Details. The properties of the initial WP and the grid parameters used for the numerical calculations are listed in Table 1. The initial state-selected integral reaction cross sections are calculated using eq 23 for a specified rovibrational state of HLi molecule. The WP is propagated for a total of $\sim$ 276 fs using the CP scheme. The norm of the WP typically comes down to 2.2×10^{-3} at the end of the time propagation. Therefore, all major dynamical events are expected to be over within this time period. It is well-known that the stability of the CP scheme depends on the maximum allowed energy on the grid. For the potential energy one generally sets a cutoff value to control the stability. The angular kinetic energy on the grid depending on the j_{max} ($=N_\gamma - 1$) and J is usually large. Very large values of this kinetic energy are unphysical and the relevant wave function does not contain any components corresponding to them. In the present application, the maximum permitted value of the angular kinetic energy is therefore truncated gradually above a reasonable value.[42] All the calculations reported here are carried out with HLi in its vibrational and rotational ground state ($v = 0, j = 0$). Each WP propagation up to 276 fs on a single processor takes nearly 60 h of CPU time in a IBM P690 machine. The maximum allowed value of K (K_{max}) is considered up to 8. For instance, $K = 3$ state can couple with the $K = 2$ and $K = 4$, whereas $K = 8$ state can couple only with $K = 7$ not with $K = 9$ since $K_{max} = 8$. Similarly, $K = 0$ state can couple only with $K = 1$ because only positive values of K are considered here. The parity is included in the dynamical calculation, which is decided by the $(-1)^{J+p}$ value.

The convergence of the reaction probability results up to the total energy $E \sim 0.84$ eV (collision energy ~ 0.75 eV and for each J and K values is explicitly checked with respect to the numerical parameters given in Table 1. Partial wave contribution up to $J = 30$ is required to obtain the converged cross section results. This can be estimated from the J dependence of the degeneracy weighted reaction probability for the channel R1 and R2 shown in parts a and b of Figure 1, respectively. It can be seen from the figure that the partial wave contribution increases with increasing energy. Typically, we find about 10%

TABLE 1: Numerical Grid Parameters and Properties of the Initial Wavefunction Used in the Present Study

parameter	value	description
$N_R/N_r/N_\gamma$	128/64/48	no. of grid points
R_{min}/R_{max}	1.0/18.78	extension of the grid along R
r_{min}/r_{max}	1.0/8.56	extension of the grid along r
$\Delta R/\Delta r$	0.14/0.12	grid spacings along R and r
r_d	5.44	location of the dividing surface in the product channel
R_{mask}/r_{mask}	13.46/5.68	starting point of the masking function
R_0	12.0	initial location of the center of the GWP in the coordinate space
V_{cut} (eV)	3.0	maximum potential energy cutoff
E_{trans} (eV)	0.55	initial translational kinetic energy
δ	0.3	initial width parameter of the GWP
Δt (fs)	0.135	length of the time step used in the WP propagation
T (fs)	275.8	total propagation time

error in the reaction probability results for some energies at higher J (>18) values.

To this end we mention that the convergence of the results with respect to K has been verified. While the cross section results for the depletion channel show a good convergence behavior over the reported energy range, that for the exchange channel is relatively poor beyond a collision energy of $\sim$0.65 eV. The latter may be attributed to the possible shortcomings of the underlying PES employed in this study.

III. Results and Discussion

In this section, we present and discuss the results obtained for H + HLi scattering with the theoretical formalism described above and compare them with the same obtained in our previous study[5] using the JS[18,19] and the CS approximations.[3,4] The reaction probabilities are reported here for collision energies up to 0.75 eV. The reaction cross sections and thermal rate constants are calculated by averaging these probability results over all partial wave contributions.

A. Reaction Probability. The initial state-selected and energy resolved reaction probability as a function of the total energy E are plotted in Figure 2 for the total angular momentum, $J = 1$ and for $K = 0$, 1. The reaction probabilities for the HLi depletion (R1) and the H-exchange (R2) channels are shown in panels a and b, respectively. In each panel, the CC reaction probabilities are shown and compared with the CS results[5] for each values of J and K. The latter are distinguished in terms of different line types in panel b.

The initial and most probable collision energy of the GWP is chosen to be 0.55 eV and the total energy is measured relative to the minimum of the HLi potential. The reaction probabilities pertinent to a channel is calculated by integrating the reactive flux flowing into it. As stated before, the two channels above are distinguished by comparing the internuclear distances of the product H_2 and HLi molecules. The CC reaction probabilities reported here are calculated at an energy interval of 0.005 eV and summed over all open vibrational (v') and rotational (j') levels of the product molecule at a given energy. The channel specific reaction probabilities for $J = 0$ and for $J \neq 0$ (within the CS approximation) are discussed in refs 5 and 16, where the results indicated sharp resonance structures at low energies (near the onset) for both the channels. The resonances are found to be less pronounced at high energies. Also the signature of resonances gradually disappears for higher values of J. We discussed and characterized some of these resonance structures in a subsequent study, for $J = 0$[17] as well as for $J \neq 0$ including the CC.[22]

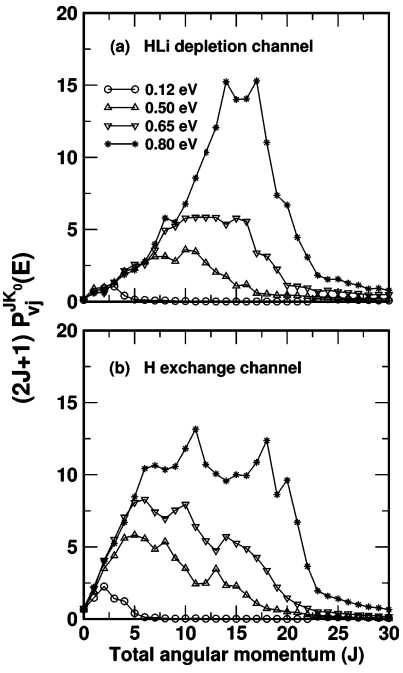

Figure 1. Weighted CC partial-wave contributions to the cumulative reaction probability and integral reaction cross sections of the R1 (panel a) and R2 (panel b) channels at various values of collision energy (indicated in panel a).

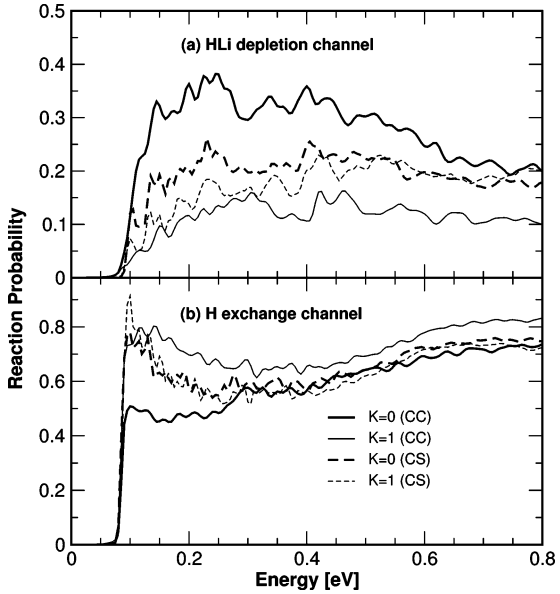

Figure 2. H + HLi ($v = 0$, $j = 0$) reaction probabilities as a function of the total energy (H−HLi translational + HLi rovibrational) for the total angular momentum $J = 1$ and for $K = 0$, 1 calculated using the CC and the CS model for the HLi depletion (panel a) and H-exchange (panel b) channels. The different line types are identified in panel b. The energy is measured relative to the minimum of the HLi potential which sets the interaction potential to zero for $R \rightarrow \infty$.

The CS calculations are carried out for a fixed value of the K quantum number, whereas in the exact (CC) calculations K is a variable quantity and is allowed to vary between 0 to $min(J, K_{max})$. A comparison of the two probability results (CS vs CC) in Figure 2, parts a and b, reveals no noticeable effects of CC on the resonance oscillations in the reaction probability curves. Resonance oscillations are only mildly quenched in the CC results. However, as observed before[22] and also revealed by the present results, the resonances tend to become broader when CC is included in the dynamics. The reaction probabilities for the H-exchange channel are generally higher than the HLi depletion channel over the studied energy range. The resonances in the CC results do survive at lower energies near the onset of the reaction even for moderate values of J. The DMJ PES[8] does not have a barrier and therefore, H + HLi reaction does not have a threshold on this PES, this is observed in the $J = 0$ reaction probabilities.[16] However, for $J \neq 0$ collisions, the reaction acquires a threshold energy due to the presence of a centrifugal barrier. All CC results reveal that the H-exchange channel is dominant over the HLi depletion channel even for the higher values of J.

The CC reaction probability results shown in Figure 2, parts a and b, when summed up for each values of K show an average of ~15% deviation from unity. Therefore ~15% of the WP flux flow into the nonreactive channel for this lower values of J and K. However, the extent of the nonreactive scattering increases with increasing values of J and K. The latter may be attributed to the increasing height of the centrifugal barrier which acts in favor of the WP flux flowing into the nonreactive channel.

In Figure 3, we show the CC reaction probabilities for various values of the total angular momentum, $J = 5$, 10, 15 and 20, for $K = 0 - min(J, K_{max})$. The identity of the probability curves is given in panel a at the upper left corner of the figure. The probabilities for the channel R1 and R2 are shown in the left and right columns of the figure, respectively. It can be seen that the reaction path R2 is generally preferred over R1 within the reported energy range. For $J = 5$, the reaction probability curves show some resonance oscillations which survive at low energies for both the channels. These resonance oscillations are gradually lost with increasing values of J (cf. Figure 3, parts c and d). This is consistent with our earlier observations that the resonances tend to become broader with increasing J. The onset of the reaction also shifts to higher energies with increasing J, because of an increase in the height of the centrifugal barrier.

B. Reaction Cross Section and Thermal Rate Constant. The initial state-selected and channel specific integral reaction cross section, as a function of collision energy in H + HLi ($v = 0, j = 0$) scattering is shown in Figure 4. These cross sections are obtained by summing up different partial wave contributions with appropriate weight to the reaction probability using eq 23. For each J values, K varied from 0 to min (J, K_{max}), with $K_{max} = 8$ up to $J = 20$ and $K_{max} = 4$ for further higher J values. The cross sections for both the R1 and R2 channels obtained in the CC and CS models are shown, and distinguished by different line types (indicated in the panel) in Figure 4. For a clearer representation, the cross sections at low collision energies are shown on an enlarged scale and included as an inset in Figure 4. It can be seen from Figure 4 that the CS results are generally larger than the CC results for both the channels at low collision energies. The overall pattern of variation of the cross section results is similar in both the models. This indicates no dramatic influence of the CC on the reaction mechanism. The weak resonance features seen in the CS results near the onset of both

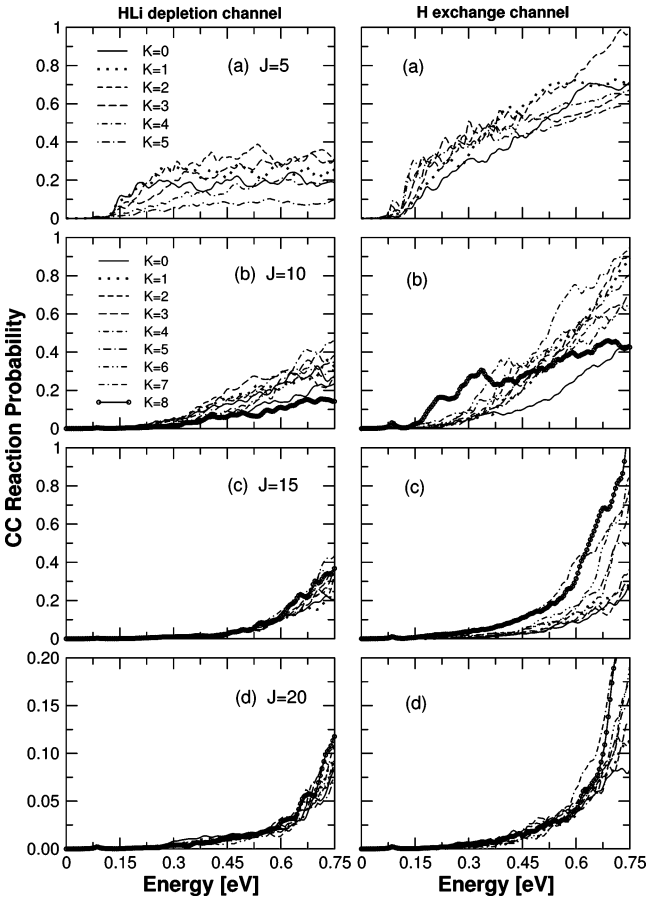

Figure 3. Same as in Figure 2. The CC reaction probabilities are shown for different J and K values (indicated in each panel). The different line types are identified in panels a and b, and the probabilities for the R1 and R2 channels are shown in the left and right column of the figure, respectively. The line types in panels c and d have the same meaning as in panel b.

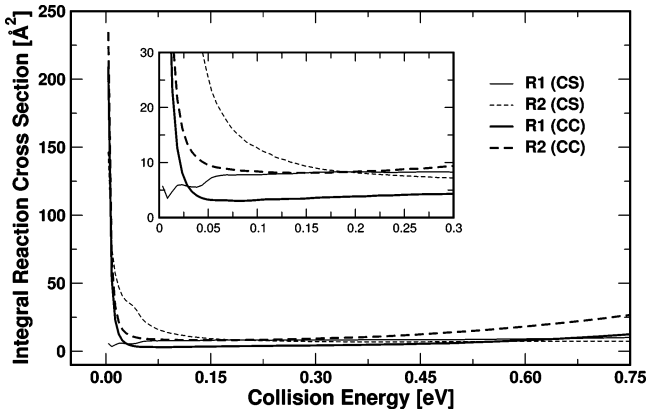

Figure 4. Initial state-selected integral reaction cross sections for the H + HLi ($v = 0, j = 0$) collisions as a function of the (H,HLi) collision energy for the R1 and R2 channels, obtained from the CC and CS models, are shown in the panel. The different line types are identified by suitably labeling them in the panel. The cross sections are shown on an enlarged scale (as inset) in panel in order to clearly reveal the effects of CC on the reaction dynamics.

the channels are absent in the CC results. The reaction cross section values are much larger near the onset of both the channels R1 and R2 and suddenly decrease to lower values with increasing collision energy. This is consistent with the characteristics of a barrierless reaction.[1] A large decrease in the reaction cross section beyond the onset implies a substantial flow of WP flux to the NR channel.

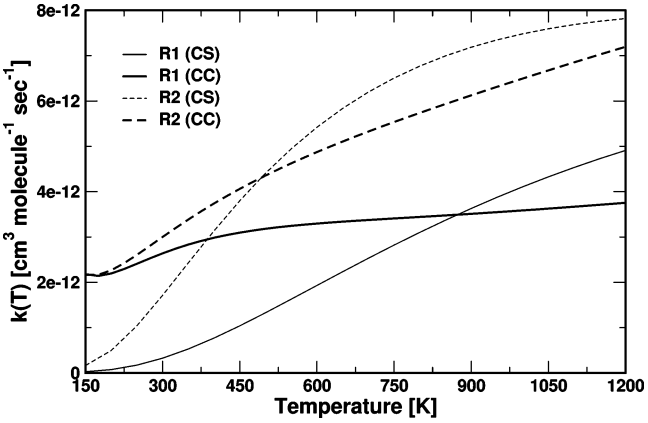

Figure 5. Initial state-selected thermal rate constants for the H + HLi ($v = 0$, $j = 0$) reaction. The rate constant results for both the R1 and R2 channels calculated using the CC and CS models are shown in the panel. Different rate constant curves are identified by labeling them in the panel.

The initial state-selected thermal rate constants for the (R1) and (R2) channels up to 1200 K calculated using eq 24 are shown in Figure 5. Both the CC and CS rate constants are plotted and the convergence of the results in the given temperature range is explicitly checked. The curves are identified by labeling each one of them in the panel. We note that these represent the initial state-selected rate constants pertinent to HLi ($v = 0$, $j = 0$). The CS results are modified slightly compared to our earlier report[5] as a more exact expression of the vibrational and rotational partition functions are used here [see eqs 25c and 25d]. The behavior of the rate constant curves are analogous to those reported by Defazio et al.[20] obtained using the state-to-state reaction probability and a JS approximation. It can be seen from Figure 5 that the CS rate constants are smaller than the CC rate constants at low temperatures: up to ~850 K for the R1 channel and up to ~450 K for the R2 channel. At high temperatures, the CS results are consistently larger than the CC results and the difference is more in the case of R2 than R1 channel. The Coriolis terms, therefore, effectively reduces the reaction rate constants at higher temperatures for both the R1 and R2 channels. The pattern of variation of the rate constant results with temperature reveals a substantial deviation from the Arrhenius behavior for both the channels within this temperature range. This point is also discussed at length by Defazio et al.[20] The convergence of the present rate constant results is improved compared to our previous CS results.[5] A close look at the values of the reaction rate for both the channels clearly indicates that the R2 channel is preferred over the R1 channel in the given temperature range. At lower temperature the two rate constants are close to each other. We do not extrapolate them to ultracold conditions as the present cross section results are not obtained in such conditions.

The initial state-selected thermal rate constant for the depletion reaction (R1) shown above are fitted to the functional form, $k(T) = aT \exp(-bT)$, as suggested by Stancil et al.[10] in their kinetic model of lithium reactions in the primordial gas clouds. The values of a and b obtained from the present fits are given in Table 2. The given parameters represent the rate constants well, beyond room temperature. It can be seen from Table 2 that the fit parameters obtained from the CC results are larger than those obtained from the CS results for the R1 channel. The empirical results of Stancil et al.[10] and also the QCT results of Dunne et al.[8] are also given in the table. The difference between our results and that of the latter authors is presumably due to the initial state-averaged nature of their rate constant data.

TABLE 2: The Present CC Rate Constant Results for the HLi Depletion Channel Fitted to the Functional Form $k(T) = AT \exp(-BT)$[a]

method	a [cm^3 molecule^{-1} s^{-1} K^{-1}]	b [K^{-1}]
CC (present)	1.26×10^{-14}	0.0013
CS (revised)[5]	2.19×10^{-15}	0.0006
Stancil et al.[10]	6.60×10^{-14}	0.0000
Dunne et al.[8]	8.40×10^{-13}	0.0004

[a] The numerical values of the fit parameters a and b are listed along with the available literature results.

At this point we would like to make a few remarks on the issue raised by one of the reviewers. The large energy release (~ 2.09 eV) in the exothermic path (R1) is sufficient to cause electronic excitation of Li atom. It is discussed by Chen et al.[43,44] that the reverse endoergic reaction, $Li(2^2P_J) + H_2 \rightarrow LiH(X\ ^1\Sigma^+) + H$, favors an insertion type of mechanism at the C_{2v} arrangements of the reactant Li and H_2. In the entrance channel of this process a curve crossing between the 1A′ and 2A′ electronic states occurs at a stretched geometry of the reagent H_2 in the attractive region of the 2A′ PES. The reaction dynamics therefore proceeds via a nonadiabatic path; the Li + H_2 collision initially takes place along the excited 2A′ surface in the entrance channel and then it leads to the formation of products LiH + H in the 1A′ electronic ground state via nonadiabatic transitions.[44] The present results are also expected to be influenced by such a mechanism, and would result into a reduction of the reported depletion/exchange reaction cross sections by further branching into the electronically excited 2A′ PES. A theoretical investigation of this aspect requires the detailed PESs and their nonadiabatic coupling surface and is beyond the scope of the present investigation.

IV. Summary and Conclusion

We presented a theoretical account of the H + HLi reactive scattering dynamics investigated in full-dimensions with the aid of a time-dependent WP approach and an ab initio PES of the ground electronic state of the system.. The present study represents an extension of our previous study on the system carried out in reduced dimensions using the CS approximation. The effect of the Coriolis coupling on the initial state-selected integral reaction cross sections and thermal rate constants is reported.

The calculations of reaction probability are carried out up to $J = 30$, required to obtain the converged reaction cross section up to a collision energy of ~ 0.75 eV. The coupling between the neighboring K states are considered up to $K_{max} = 8$. The resonance oscillations in the reaction probability curve tend to become broader on inclusion of the CC terms. The integral reaction cross sections are generally lower in the CC model when compared to the same obtained from the CS model, for both the R1 and R2 channels. The integral reaction cross sections of the H-exchange channel R2 are larger than those of the HLi depletion channel R1. The cross sections does not have a threshold indicating the feature of a barrierless reaction which is again reflected in substantial deviation of the thermal rate constant results from the Arrhenius behavior. The rate constants for both the channels are very close to each other at low temperatures and the exchange rate is more than the depletion rate at high temperatures. The CC lowers the rate constant of both the channels at high temperatures when compared to the CS results.

Acknowledgment. This study is in part supported by a research grant from the Council of Scientific and Industrial Research (CSIR), New Delhi, India (Grant No. CSIR-01(1917)/04/EMR−II). R.P. acknowledges the CSIR for a Senior Research Fellowship. We thank the University Grants Commission and the Department of Science and Technology for the computational facilities provided under the University with potential for the excellence and the high performance computational facility program, respectively, in the University of Hyderabad.

References and Notes

(1) Clary, D. C. *The theory of Chemical Reaction Dynamics*; Reidel: Boston, MA, 1986. Levine, R. D.; Bernstein, R. B. *Molecular Reaction Dynamics and Chemical Reactivity*; Oxford University Press: Oxford, U.K., 1987. Wyatt, R. E.; Zhang, J. Z. H. *Dynamics of Molecules and Chemical Reactions*; Marcel Dekker: New York, 1996. Althorpe, S. C.; Clary, D. C. *Annu. Rev. Phys. Chem.* **2003**, *54*, 493.

(2) Zhang, J. Z. H. *Theory and Application of Quantum Molecular Dynamics*; World Scientific: Singapore, 1999.

(3) Pack, R. T. *J. Chem. Phys.* **1974**, *60*, 633. McGuire, P.; Kouri, D. J. *J. Chem. Phys.* **1974**, *60*, 2488.

(4) Judson, R. S.; Kouri, D. J.; Neuhauser, D.; Baer, M. *Phys. Rev. A* **1990**, *42*, 351. Baram, A.; Last, I.; Baer, M. *Chem. Phys. Lett.* **1993**, *212*, 649.

(5) Padmanaban, R.; Mahapatra, S. *J. Chem. Phys.* **2004**, *121*, 7681. Erratum: *J. Chem. Phys.* **2005**, *122*, 029902.

(6) Wang, D.; Yang, M.; Han, K.-Li; Zhang, D. *J. Theor. Comput. Chem.* **2005**, *4*, 857. Chu, T.-S.; Han, K.-Li *J. Phys. Chem. A* **2005**, *109*, 2050. Chu, T.-S.; Lu, R.-F.; Han, K.-Li; Tang, X.-N.; Xu, H.-F.; Ng, C. Y. *J. Chem. Phys.* **2005**, *122*, 244322.

(7) Morari, C.; Jaquet, R. *J. Phys. Chem. A* **2005**, *109*, 3396.

(8) Dunne, L. J.; Murrell, J. N.; Jemmer, P. *Chem. Phys. Lett.* **2001**, *336*, 1.

(9) Lepp, S.; Shull, J. M. *Astrophys. J.* **1984**, *280*, 465.

(10) Stancil, P. C.; Dalgarno, A. *Astrophys. J.* **1997**, *479*, 543. Stancil, P. C.; Lepp, S.; Dalgarno, A. *Astrophys. J.* **1996**, *458*, 401.

(11) Bodo, E.; Gianturco, F. A.; Martinazzo, R. *Phys. Rep.* **2003**, *384*, 85.

(12) Dalgarno, A.; Fox, J. L. in *Unimolecular and Bimolecular Reaction Dynamics*; Ng, C. Y.; Baer, T.; Powis, I., Eds.; Wiley: Chichester, U.K., **1994**, 1. Signore, M.; et al. *Astrophys. J. Suppl. Ser.* **1994**, *92*, 535. Maoli, R.; Melchiorri, F.; Tosti, D. *Astrophys. J.* **1994**, *425*, 372.

(13) Dubrovich, V. K. *Astron. Lett.* **1993**, *19*, 53.

(14) Clarke, N. J.; Sironi, M.; Raimondi, M.; Kumar, S.; Gianturco, F. A.; Buonomo, E.; Cooper, D. L. *Chem. Phys.* **1998**, *233*, 9.

(15) Kim, K. H.; Lee, Y. S.; Ishida, T.; Jeung, G.-H. *J. Chem. Phys.* **2003**, *119*, 4689.

(16) Padmanaban, R.; Mahapatra, S. *J. Chem. Phys.* **2002**, *117*, 6469.

(17) Padmanaban, R.; Mahapatra, S. *J. Chem. Phys.* **2004**, *120*, 1746.

(18) Bowman, J. M. *Adv. Chem. Phys.* **1985**, *61*, 115; *J. Phys. Chem.* **1991**, *95*, 4960.

(19) Mielke, S. L.; Lynch, G. C.; Truhlar, D. G.; Schwenke, D. W. *J. Phys. Chem.* **1994**, *98*, 8000. Zhang, D. H.; Zhang, J. Z. H. *J. Chem. Phys.* **1999**, *110*, 7622.

(20) Defazio, P.; Petrongolo, C.; Gamallo, P.; Gonzaález, M. *J. Chem. Phys.* **2005**, *122*, 214303.

(21) Gray, S. K.; Balint-Kurti, G. G. *J. Chem. Phys.* **1998**, *108*, 950.

(22) Padmanaban, R.; Mahapatra, S. *J. Theor. Comput. Chem.* , in press.

(23) Pack, R. T.; Parker, G. A. *J. Chem. Phys.* **1987**, *87*, 3888.

(24) Meijer, A. J. H. M.; Goldfield, E. M. *J. Chem. Phys.* **1998**, *108*, 5404. Goldfield, E. M.; Meijer, A. J. H. M. *J. Chem. Phys.* **2000**, *113*, 11055. Carroll, T. E.; Goldfield, E. M. *J. Phys. Chem. A* **2001**, *105*, 2251.

(25) Lin, S. Y.; Guo, H. *J. Phys. Chem. A* **2004**, *108*, 2141.

(26) Leforestier, C. *J. Chem. Phys.* **1991**, *94*, 6388.

(27) Goldfield, E. M.; Gray, S. K. *Comput. Phys. Commun.* **1996**, *98*, 1 and references therein. Chen, R.; Guo, H. *Comput. Phys. Commun.* **1999**, *119*, 19.

(28) Edmonds, A. R. *Angular Momentum in Quantum Mechanics*; Princeton University: Princeton, NJ, 1960.

(29) Zare, R. N. *Angular momentum*; John Wiley & Sons: New York, 1988.

(30) Condon, E. U.; Shortley, G. H. *The Theory of Atomic Spectra*; Cambridge University Press: Cambridge, U.K., 1935.

(31) Colbert, D. T.; Miller, W. H. *J. Chem. Phys.* **1992**, *96*, 1982.

(32) Tal-Ezer, H.; Kosloff, R. *J. Chem. Phys.* **1984**, *81*, 3967.

(33) Kosloff, D.; Kosloff, R. *J. Comput. Phys.* **1983**, *52*, 35.

(34) Light, J. C.; Hamilton, I. P.; Lill, J. V. *J. Chem. Phys.* **1985**, *82*, 1400. Bačić, Z.; Light, J. C. *Annu. Rev. Phys. Chem.* **1989**, *40*, 469.

(35) Corey, G. C.; Lemoine, D. *J. Chem. Phys.* **1992**, *97*, 4115.

(36) Press, W. H.; Flannery, B. P.; Teukolsky, S. A.; Vetterling, W. T. *Numerical Recipes in Fortran: The Art of Scientific Computing*, 2nd ed.; Cambridge University Press: New York, 1986; p 125.

(37) Mahapatra, S.; Sathyamurthy, N. *J. Chem. Soc., Faraday Trans.* **1997**, *93*, 773.

(38) Seideman, T.; Miller, W. H. *J. Chem. Phys.* **1991**, *96*, 4412. *J. Chem. Phys.* **1992**, *97*, 2499. Manthe, U.; Miller, W. H. *J. Chem. Phys.* **1993**, *99*, 3411.

(39) Miller, W. H. *J. Phys. Chem.* **1998**, *102*, 793 and references therein.

(40) Zhang, D. H.; Zhang, J. Z. H.; Zhang, Y. C.; Wand, D. Y.; Zhang, Q. G. *J. Chem. Phys.* **1995**, *102*, 7400. Kalyanaraman, C.; Clary, D. C.; Sathyamurthy, N. *J. Chem. Phys.* **1999**, *111*, 10910.

(41) McQuarrie, D. A. *Statistical Mechanics*; University of California: Davis, CA, 2000.

(42) Göğtas, F.; Balint-Kurti, G. G.; Offer, A. R. *J. Chem. Phys.* **1996**, *104*, 7927.

(43) Chen, J.-J.; Hung, Y.-M.; Liu, D.-K.; Fung, H.-S.; Lin, K.-C. *J. Chem. Phys.* **2001**, *114*, 9395.

(44) Chen, J.-J.; Lin, K.-C. *J. Chem. Phys.* **2003**, *119*, 8785.